Quantitative simulation of photoacoustic signals using finite element modelling software

Bertrand Parvitte · Christophe Risser ·
Raphael Vallon · Virginie Zéninari

Abstract This paper aims to demonstrate the quantitative simulation of photoacoustic signals using finite element modelling software. The software Comsol Multiphysics is used to calculate the response of a differential Helmholtz resonator cell previously modeled using an electrical analogy. Quality factors and resonance frequencies are compared with experimental ones. Moreover, for the first time, the absorption coefficient of the gas sample and the laser intensity are also used to quantitatively predict photoacoustic signal that can be obtained in such a configuration.

1 Introduction

Photoacoustic (PA) spectroscopy has proven to be a very sensitive method for gas monitoring [1]. The PA technique consists of sending modulated radiation into a sample gas cell containing a microphone. Any absorbed radiation will be, in general, converted to thermal energy of the gas due to collisions of molecules, thus leading to a modulated pressure detectable with a microphone. As any spectroscopic system, a PA detector presents the main advantage of being highly selective. Moreover, PA sensors are the robust devices that can easily be implemented for in situ monitoring. Thanks to resonant cells and differential measurement techniques; PA sensors have shown excellent sensitivities on the level of part-per-billion (ppb) for most atmospheric gases [2–5]. These results are comparable to those of other apparatus, such as multipass cells or cavity enhanced absorption spectroscopy techniques, but with a generally simpler set-up. Finally, PA sensors present the advantages of a high dynamic range and the possibility to work at atmospheric pressure.

To improve the sensitivity of the system, resonant cell schemes can be used exploiting most of the time radial, azimuthal or longitudinal resonance of acoustic waves. The cell that will be quantitatively modelled in the present paper is based on a different scheme: resonance is obtained by differential Helmholtz resonance [6]. This type of resonator has been used by several teams to develop trace gas sensors [7–10]. Two volumes V_a and V_b linked by two capillaries form this PA cell. The gas in the capillaries moves like a piston, compressing gas in one volume whereas dilating it in the other. Consequently, acoustic waves are opposite in phase at resonance and by measuring it with two microphones (one in each volume), differential measurement is obtained: the difference of the two signals eliminates a great part of the acoustic noise and rises by a factor 2, the acoustic signal itself. The two capillaries enable to do flow measurements, as each of them is supplied with a valve, linked on one side to vacuum pumping system, on the other to atmosphere.

In photoacoustic spectroscopy, the light must be modulated at acoustic frequency to generate a signal in the cell. In the case of amplitude modulation, $W(\omega, t)$ corresponds to the mean power in the cell, if we assume that $W(\omega, t) = W_m(1 + \exp i\omega t)$ where ω is the angular frequency. PA signal is linked to Beer–Lambert law [1]:

$$S_{PA} = \frac{RW}{L}(1 - \exp(-\alpha L)) \tag{1}$$

where R is the total cell response, W the laser power, L the cell length and α the absorption coefficient of the gas sample.

B. Parvitte · C. Risser · R. Vallon · V. Zéninari (✉)
Groupe de Spectrométrie Moléculaire et Atmosphérique,
UMR CNRS 7331, UFR Sciences Exactes et Naturelles,
Université de Reims Champagne-Ardenne, Moulin de la Housse,
BP 1039, 51687 Reims Cedex 2, France
e-mail: virginie.zeninari@univ-reims.fr

For low concentrations of absorbing molecules, the PA signal is then equal to:

$$S_{PA} = RW\alpha \tag{2}$$

The total response of the PA system is given by [11] :

$$R = \frac{(\gamma - 1)LQR_m}{\omega V_c} = R_c R_m \tag{3}$$

where γ is the ratio of the specific heat at constant pressure C_p to specific heat at constant volume C_v, Q the quality factor of the resonant cell, R_m the microphone sensitivity and V_c the cell volume. R_c characterizes the acoustical response of the cell. Usually, this total cell response is not calculated using Eq. 3, but is obtained using calibrated mixtures in the cell and measuring the obtained photoacoustic signal [12, 13]. This calibration procedure may be a burdensome work that needs expensive certified mixtures. Moreover this task may be realized only when the photoacoustic cell is constructed. For this two reasons, it is very interesting to quantitatively model the response of a photoacoustic cell. This paper will demonstrate the possibility to determine photoacoustic cell constant without any calibration procedure, and to predict the absolute photoacoustic signal obtained in various configuration using the finite element modelling (FEM) software Comsol Multiphysics.

2 Description of a differential Helmholtz resonant cell

Helmholtz resonances have been first experimentally observed in the analysis of solid samples with photoacoustic cells designed to separate the microphone cavity from the sample chamber [14, 15]. Simple system models, based on equation for a driven harmonic oscillator [16] and acoustic analogy to the electric circuit approach [17, 18], predict with acceptable accuracy both the experimentally determined responses of Helmholtz resonator as function of frequency and values of acoustic quality factor Q. Compared to other resonators, the Helmholtz arrangement has the advantages of using cells of small volumes with low resonance frequency, and the possibility to enhance the S/N ratio using differential schemes. The differential Helmholtz resonant cell presented here is simple in design and consists of two cell volumes connected together by thin capillaries. A 3D view of the cell is presented in Fig. 1.

To investigate all parameters of the Helmholtz resonance and the feasibility of the flow measurement, we have built several identical Pyrex PA cells. Each cell is equipped with low-cost commercial electret microphones, Knowles EK3024. The cells have BaF$_2$ windows mounted at Brewster angle. The Helmholtz configuration is obtained by connecting the cells to each other by two identical Pyrex
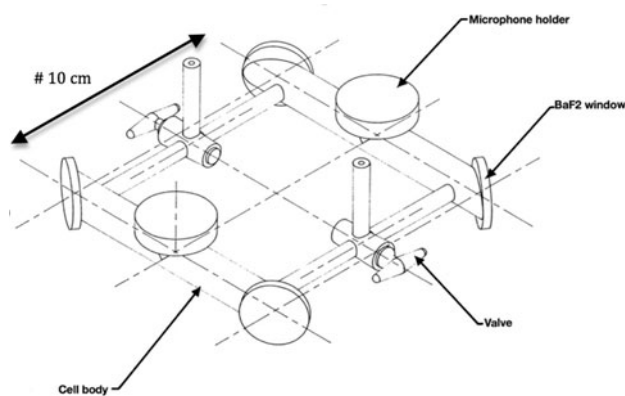

Fig. 1 Three-dimensional view of the glass PA cell

Table 1 Geometrical parameters of the DHR cell

Parameter	Value
Length of the cell Lc (m)	0.102
Cell diameter Dc (m)	0.0108
Length of the capillaries Lcap (m)	0.071
Capillaries diameter Dcap (m)	0.00206
Length of the valves Lv (m)	0.013
Valves diameter Dv (m)	0.0015

capillaries with two-way vacuum valves to form a bilateral symmetric design. The geometrical parameters of the cell are summarized in Table 1.

The experimental characterization of the cells was performed using a continuous wave SAT C7 $^{18}O^{12}C^{18}O$ waveguide laser, emitting on 9P20 line with a mean power around 0.5 W, chopped by a high precision mechanical chopper EG&G, model 197, at frequencies from 20 to 300 Hz. The laser beam passes through the first cell of the photoacoustic detector and is directed to a power meter. Emission wavelength is checked by a CO$_2$ spectrum analyzer Optical Engineering.

The two-way vacuum valves allow to operate the PA cell either in non-resonant mode where the excited cell is isolated from the other and the two capillaries are closed, or in resonant mode where one or both capillaries are open. In non-resonant mode, the measured signal U$_0$ is the response of the microphone located in the excited cell. In resonant mode, the signals U$_a$ and U$_b$ correspond, respectively, to the response of the microphone (a) located in the excited cell and the microphone (b) in the non-excited cell. The configuration is named Helmholtz Resonator (HR) if the microphone signals in each cell (U$_a$ and U$_b$) are measured separately, and Differential Helmholtz Resonator (DHR) if the difference between the microphone signals U$_a$ − U$_b$ is measured. Fig. 2 presents a schematic representation of the two possibilities of use of the PA cell.

Fig. 2 Schematic representation of the non-resonant photoacoustic cell when capillaries are closed (a), and of the Helmholtz resonator obtained by connecting the two identical cells with the two capillaries (b)
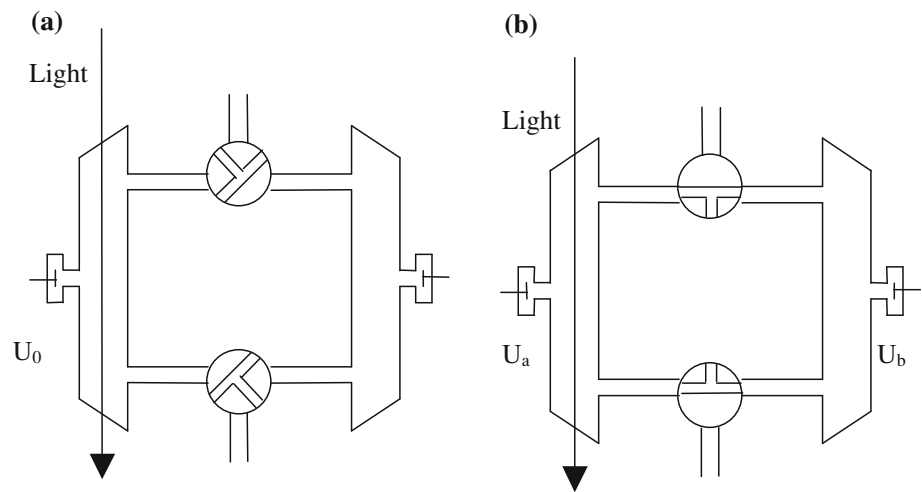
The characteristics of the cell (sensitivity or responsivity as function of frequency, pressure and concentration of absorbing gas molecules) in non-resonant, HR and DHR configurations were experimentally determined using ethylene in the vapor phase (Air Liquide) diluted in N_2 (Air Liquide). We did not have certified mixtures, so the mixtures of the given concentrations were prepared in a vacuum tank and were kept for 3 or 4 h before the measurements. The amplitudes and phases of the photoacoustic signals U_0, U_a, U_b, $U_a - U_b$ were measured by two lock-in amplifiers (EG&G, model 5301), with 1s integration time for several ethylene concentrations and for several total pressure. These measurements have been detailed in [6], and compared to simulations based on electric analogy. A quantitative good agreement between measurements and simulations has been found provided, we add a supplementary loss term in the electric analogy modelization. This parameter was determined by fitting the simulation to measurements for one ethylene concentration, and was found to be correct for all other concentrations.

The need for this empirical parameter strongly limits the use of electric analogy for PA cell shape and response optimization. Although some more complex models have been developed based on electrical analogy (Extended Helmholtz Resonator [17], Matrix formalism [19]), they also require some empirical adjustments.

3 Modelization of PA cells

3.1 Description of sound generation

The theoretical description of sound generation in photoacoustic cells has been given in the 70s by several authors [11, 20], and is summarized here. According to [21], the heat produced in a photoacoustic cell by light absorption represents the source for sound wave. Therefore, a corresponding source term has to be added to the Helmholtz equation:

$$\nabla^2 p(\mathbf{r}, \omega) + k^2 p(\mathbf{r}, \omega) = i\omega \frac{\gamma - 1}{c^2} H(\mathbf{r}, \omega) \qquad (4)$$

where p is the Fourier transform of the acoustic pressure, $k = \omega/c$ and c is the sound velocity. Assuming that the absorbing transition is not saturated, and that the modulation frequency is considerably smaller than the relaxation rate of the molecular transition, the relation $H(\mathbf{r}, \omega) = \alpha I(\mathbf{r}, \omega)$ applies where $I(\mathbf{r}, \omega)$ is the Fourier transformed intensity of the electromagnetic field.

It is well-know that the solution of the inhomogeneous wave equation can be expressed as the superposition of the acoustic modes of the photoacoustic cell:

$$p(\mathbf{r}, \omega) = \sum_j A_j(\omega) p_j(\mathbf{r}) \qquad (5)$$

The modes $p_j(\mathbf{r})$ and the corresponding eigenfrequencies $\omega_j = ck_j$ can be obtained by solving the homogeneous Helmholtz equation:

$$\nabla^2 p(\mathbf{r}) + k^2 p(\mathbf{r}) = 0 \qquad (6)$$

It is assumed that the walls of the photoacoustic cell are sound hard, which leads to the boundary condition:

$$\frac{\partial p}{\partial n} = 0 \qquad (7)$$

i.e. the normal derivative of the pressure is zero at the boundary. To use Eq. 5, it is necessary to normalize the modes according to

$$\int_{V_c} p_i^* p_j dV = V_c \delta_{ij} \qquad (8)$$

where V_c denotes the volume of the photoacoustic cell and p_i^* the complex conjugate of p_i. When the acoustic modes p_j

can be determined, the amplitude for each mode is expressed as

$$A_j(\omega) = i \frac{A_j \omega}{\omega^2 - \omega_j^2 + i\omega\omega_j/Q_j} \tag{9}$$

with

$$A_j = \frac{\alpha(\gamma - 1)}{V_c} \int_{V_c} p_j^* I dV \tag{10}$$

and

$$1/Q_j = 1/Q_j^v + 1/Q_j^{s_\kappa} + 1/Q_j^{s_\eta} \tag{11}$$

The inhomogeneous Helmholtz equation (Eq. 4) does not contain the terms that account for loss. Loss effects are included via the introduction of quality factors Q_j in the amplitude formula (9). Several loss mechanisms occur in photoacoustic cells: volume loss, thermal and viscosity surface losses. Following [11], volume loss is simply due to the energy transferred from the acoustic wave to thermal energy through heat conduction and through the viscosity:

$$1/Q_j^v = \frac{\omega_j}{c} \left[l_\eta + (\gamma - 1) l_\kappa \right] \tag{12}$$

where l_η and l_κ are characteristic lengths, respectively, defined by

$$l_\eta = \frac{4}{3} \frac{\eta}{\rho c} \tag{13}$$

$$l_\kappa = \frac{\kappa}{\rho C_p c} \tag{14}$$

with η being the viscosity and κ the thermal conductivity. ρ represents the gas density. The surface loss occurs in a thin region near the walls that is composed of two layers of thicknesses d_κ and d_η given by :

$$d_\kappa = \sqrt{\frac{2\kappa}{C_p \rho \omega_j}} \tag{15}$$

$$d_\eta = \sqrt{\frac{2\eta}{\rho \omega_j}} \tag{16}$$

Near the wall, the expansion and contraction of the gas are isothermal due to the greater thermal conductivity of the wall, whereas they are adiabatic far from the walls. Acoustic losses from heat conduction occur in the layer of thickness d_κ where the gas behavior is partly adiabatic and partly isothermal.

$$1/Q_j^{s_\kappa} = \frac{1}{2} (\gamma - 1) \frac{d_\kappa}{V_c} \int_{S_c} |p_j|^2 dS \tag{17}$$

Similarly, at the wall surfaces, the tangential component of the acoustic velocity is zero because of the viscosity, while far from the wall, it is proportional to the gradient of the acoustic pressure. Viscoelastic loss occurs in the region of thickness d_η

$$1/Q_j^{s_\eta} = \frac{1}{2} \left(\frac{c}{\omega_j} \right)^2 \frac{d_\eta}{V_c} \int_{S_c} |\nabla_t p_j|^2 dS \tag{18}$$

According to this description, the first step for the determination of PA cell response is the obtention of the acoustic eigenmodes p_j, which can be done analytically only in some specific cases (cylindrical [22] or rectangular cell, for example). When the geometry of the cell is more complex, the analytical determination of the eigenmodes is not possible. The progresses in numerical methods and the availability of user friendly software using FEM open the way to direct resolution of the Helmholtz equation and to the optimization of photoacoustic cell's response. We present, here, an example of PA cell and its analysis using numerical simulation.

3.2 FEM analysis of DHR cells

FEM softwares have been used for resonant frequencies [23], eigenmodes [24, 25] and quality factors [26] determination. Baumann et al. [27] performed a careful comparison between analytical determination and FEM simulation using Comsol Multiphysics 3.5 software for a cylindrical cell, and found a good agreement for the eigenfrequencies and for the Q factors. They also performed a comparison between FEM simulation and experiment for T-shaped resonators that also shows a good agreement for eigenfrequencies and Q factors. In order to analyze our DHR cell, we built a model with Comsol 4.2 software. Only the core of Comsol is needed to perform the calculation presented, hereafter, without any specific module. The model defines the geometry of the cell and the properties of the material, and then uses an eigenvalue solver to determine the modes $p_j(\mathbf{r})$ and the associated eigenfrequency ω_j. The calculation of the amplitudes A_j and of the various losses for each eigenfrequency is then performed using the Comsol model (Eqs. 10–18). Most of the parameters needed for the evaluation of Eqs. 10–18 are related to the gas properties (density, viscosity,...), and are already defined in Comsol for various gases. Our experiments were performed using low concentration of ethylene in N_2, and we used the predefined values for N_2. Those results and the values of $p_j(\mathbf{r})$ for particular points located near the microphones positions in the actual cell are exported to matlab to evaluate Eqs. 9 and 5. This model was first used to solve the Helmholtz equation for the various geometries presented in [27]. Amplitudes, losses and frequency responses were calculated, and a very good agreement with the published values for eigenfrequencies
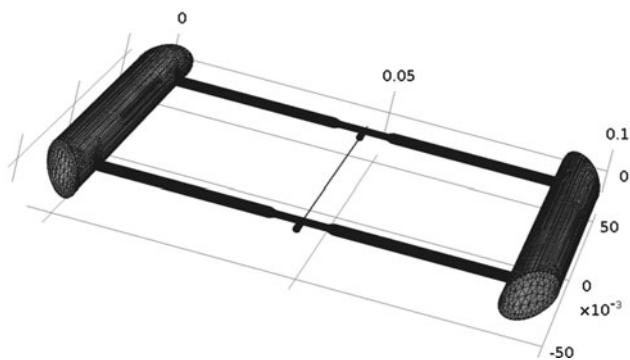
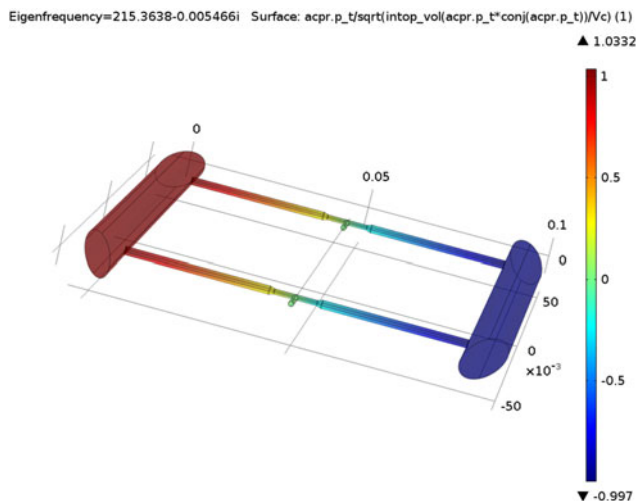**Fig. 3** Typical finite element mesh of the DHR cell

Fig. 4 Acoustic pressure repartition of the Helmholtz resonant eigenmode

and Q factors was found. In a second step, the model has been adapted to the geometry of our DHR cell. The eigenmodes of the cell have been determined, the amplitudes A_j, losses, and the frequency response have been estimated. A typical mesh of the photoacoustic DHR cell is presented on Fig. 3. The mesh is a free tetrahedral mesh and consists of about 200,000 elements. Figure 4 presents the acoustics pressure repartition for the Helmholtz eigenmode normalized using Eq. 8. For this particular eigenmode, one can observe the phase opposition for the acoustic pressure in both parts of the cell.

During the experiments, four different signals were measured versus the modulation frequency (U_a, U_b and $U_a - U_b$ in resonant mode and U_0 in non-resonant mode). The experimental resonant frequency for U_a (respectively, U_b, $U_a - U_b$) is the frequency that corresponds to the maximum of $|U_a|$ (respectively, $|U_b|$, $|U_a - U_b|$). The quality factor for U_a (respectively, U_b, $U_a - U_b$) is given by the peak value of $|U_a|/|U_0|$ (respectively, $|U_b|/|U_0|$, $|U_a - U_b|/|U_0|$). These values are summarized in the first

Table 2 Comparison between experimental and calculated values for the Helmholtz resonant frequencies and quality factors

	Measurements	Simulation
Eigenfrequency (Hz)		215.35
U_a resonant frequency (Hz)	221 ± 2	219.2
U_b resonant frequency (Hz)	209 ± 2	211.1
$U_a - U_b$ resonant frequency (Hz)	215 ± 2	215.3
U_a Quality factor	2.8 ± 0.1	2.72
U_b Quality factor	2.7 ± 0.1	2.58
$U_a - U_b$ Quality factor	5.2 ± 0.2	5.12

column of Table 2. Resonant frequencies and quality factors are derived from FEM simulation by evaluating Eq. 5 at two nodes of the mesh located, respectively, near microphone (a) and microphone (b). The quality factor for U_a (respectively, U_b, $U_a - U_b$) is obtained by dividing the resonant frequency for U_a (respectively, U_b, $U_a - U_b$) by the witdh at half maximum of the frequency response for U_a (resp. U_b, $U_a - U_b$). These values are summarized in the second column of Table 2.

All these values are in good agreement and we can conclude that the use of FEM simulation to solve the homogeneous Helmholtz equation (Eq. 6) to obtain resonance frequencies, and quality factor is satisfactory even for cell geometries that significantly differs from cylindrical or rectangular shape (Brewster angle windows, thin capillaries, etc.). Furthermore, we will demonstrate in the next part that FEM simulation can also provide accurate and quantitative value for the cell's response R_c.

4 Quantitative modelization of photoacoustic signals

In their implementation of the calculation of the amplitude associated with the eigenmodes (see Eq. 10), Baumann et al. [27] were only interested in the spatial repartition of the beam intensity:

$$I(r_\perp) = I_0 \exp\left(-2\left(\frac{r_\perp}{w}\right)^2\right) \quad (19)$$

where w is the beam radius and $r_\perp = \sqrt{y^2 + z^2}$ is the distance perpendicular to the beam axis of propagation denoted by x. An arbitrary value for the product αI_0 was

Table 3 Experimental parameters

Parameter	Value
Ethylene concentration	$\sim 4\%$
α @ $\lambda(CO_2)$	0.0166 cm^{-1}
Laser power	0.62 W
ω	1.55 mm

used in their calculations (Evaluation of Eq. 10). Instead of this arbitrary value for αI_0, the absorption coefficient α is derived from the HITRAN 2008 database [28] for our absorbing gas concentration and to express I_0 in term of the laser power P:

$$\int \int_{S_0} I_0 \exp\left(-2\left(\frac{r_\perp}{w}\right)^2\right) dy dz = P \qquad (20)$$

where S_0 is the projection of the entrance window perpendicular to x axis. Comsol multiphysics is used to perform the integration of $\exp\left(-2\left(\frac{r_\perp}{w}\right)^2\right)$ over the entrance window cross-section and to calculate I_0.

The model ran using the values of laser power and C_2H_4 concentration, corresponding to our previous measurements. Several values for the parameters A_j, Q_j^i and for the pressures $p_j(\mathbf{r})$ at the positions corresponding to the microphones in each part of the cell are then obtained. A short matlab script is used to evaluate the expressions (10) and (5) over a convenient frequency range. As the Helmholtz resonance frequency is much lower than the longitudinal, radial or azimutal resonance frequencies, only the firsts eigenmodes need to be determined. In first step, our model was used on a non-resonant geometry (corresponding to one half of the DHR cell). The comparison of simulation with measurements for this non-resonant geometry is plotted on Fig. 5. On this figure, the measured signal U_0 is normalized by the frequency response R_m of the Knowles microphones. The experimental conditions (C_2H_4 concentration and absorption coefficient, laser power...) are summarized in Table 3. A traditional 1/f dependence is observed and the agreement between experiment and simulation is very good.
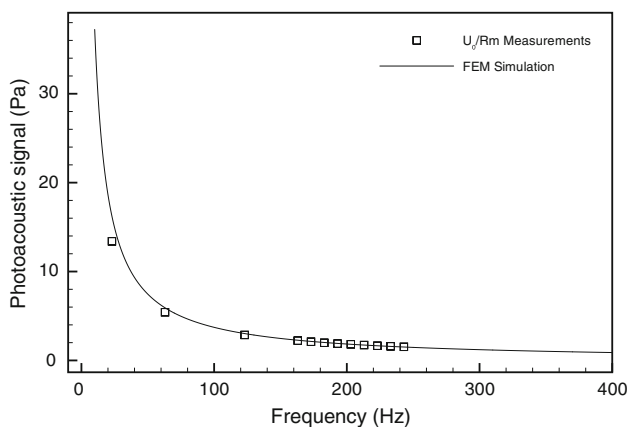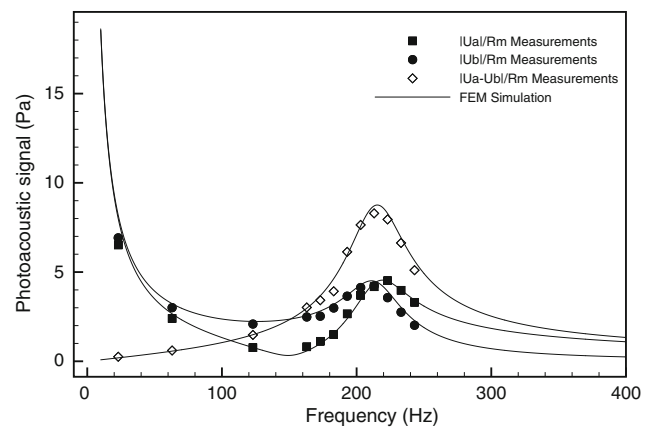

Fig. 6 Modelization of the response of the cell in resonant mode (*capillaries open*) and comparison with measurements. The experimental conditions are summarized in Table 3

In second step, the same model was used with the resonant geometry (complete cell, corresponding to both capillaries open), and the pressure wave amplitude was calculated in both the excited and the non-excited part of the cell. The comparison of simulation with measurements for the resonant geometry is plotted on Fig. 6. Again, the model perfectly fits the experimental points demonstrating the possibility to quantitatively simulate photoacoustic signal using FEM software.

5 Conclusion

This paper has demonstrated the possibility to quantitatively simulate photoacoustic signals using FEM software. After a brief report on the theoretical description of sound generation in photoacoustic cells, the modelling of a previously developed differential Helmholtz resonant cell was presented. The software Comsol Multiphysics 4.2 was used to calculate the response of DHR cell. Quality factors and resonance frequencies were compared with experimental ones demonstrating a very good agreement. The fact that the FEM calculation doesn't contain any fitted parameter may be underlined. Moreover, in the last part, the absorption coefficient of the gas and the laser intensity were used in addition to FEM simulation to quantitatively predict photoacoustic signal that can be obtained in such a configuration. This calculation has demonstrated a very good agreement with experimental data. To our knowledge, this paper is the first demonstration of a complete modelization of photoacoustic cell. This will be particularly useful for size reduction of this type of cells.

Fig. 5 Modelization of the response of the cell in non-resonant mode (*capillaries closed*) and comparison with measurements. The experimental conditions are summarized in Table 3

References

1. M.W. Sigrist, *Air Monitoring by Spectroscopic Techniques* (Wiley, New York, 1994), pp. 163–238
2. A. Grossel, V. Zéninari, B. Parvitte, L. Joly, G. Durry, D. Courtois, Infrared Phys. Technol. **51**, 95–101 (2007)
3. A. Grossel, V. Zéninari, B. Parvitte, L. Joly, G. Durry, D. Courtois, Appl. Phys. B: Lasers Opt. **88**, 483–492 (2007)
4. M.A. Gondal, M.A. Dastageer, J. Environ. Sci. Health - Part A Toxic/Hazard. Subst. Environ. Eng. **45**, 1405–1412 (2010)
5. A.A.I. Khalil, M.A. Gondal, N. Al-Suliman, Appl. Phys. B: Lasers Opt. **103**, 441–450 (2011)
6. V. Zeninari, V.A. Kapitanov, D. Courtois, Y.N. Ponomarev, Infrared Phys. Technol. **40**, 1–23 (1999)
7. S. Barbieri, J.-P. Pellaux, E. Studemann, D. Rosset, Rev. Sci. Instrum. **73**, 2458–2461 (2002)
8. M. Mattiello, M. Niklés, S. Schilt, L. Thénaz, A. Salhi, D. Barat, A. Vicet, Y. Rouillard, R. Werner, J. Koeth, Spectrochim. Acta-Part A: Mol. Biomol. Spectros. **63**, 952–958 (2006)
9. J.M. Rey, M.W. Sigrist, Rev. Sci. Instrum. **78**, 063104 (2007)
10. S. Tan, W.-F. Liu, L.-J. Wang, J.-C. Zhang, L. Li, J.-Q. Liu, F.-Q. Liu, Z.-G. Wang, Guang Pu Xue Yu Guang Pu Fen Xi/Spectrosc. Spectr. Anal. **32**, 1251–1254 (2012)
11. A. Rosencwaig, *Photoacoustics and Photoacoustic Spectroscopy* (Wiley, New York, 1980), pp. 15–71
12. G.Z. Angeli, A.M. Solym, A. Miklos, D.D. Bicanic, Anal. Chem. **64**, 155–158 (1992)
13. V. Zeninari, B. Parvitte, D. Courtois, V.A. Kapitanov, Y.N. Ponomarev, Infrared Phys. Technol. **44**, 253–261 (2003)
14. R.S. Quimby, P.M. Selzer, W.M. Yen, Appl. Opt. **16**, 2630–2632 (1977)
15. N.C. Fernelius, Appl. Opt. **18**, 1784–1787 (1979)
16. W.A. McClenny, C.A. Bennett Jr., G.M. Russwurm, R. Richmond, Appl. Opt. **20**, 650–653 (1981)
17. O. Nordhaus, J. Pelzl, Appl. Phys. **25**, 221–229 (1981)
18. J. Blitz, *Elements of Acoustics* (Butterwoth, Oxford, 1964), pp. 64–90
19. S. Bernegger, M.W. Sigrist, Infrared Phys. **30**, 125–132 (1990)
20. Y.-H. Pao, *Optoacoustic Spectroscopy and Detection* (Academic Press, San Diego, 1977), pp. 1–30
21. P.M. Morse, K.U. Ingard, *Theoretical Acoustics* (Princeton University Press, New Jersey, 1968)
22. P.M. Morse, *Vibration and Sound* (McGraw-Hill, New York, 1948), pp. 385–415
23. D.A. Heaps, P.M. Pellegrino, Proc. SPIE **6218**, 1–9 (2006)
24. B. Baumann, B. Kost, H. Groninga, M. Wolff, *Proceedings of the COMSOL Multiphysics User's Conference*, 2005
25. B. Baumann, B. Kost, H. Groninga, M. Wolff, Rev. Sci. Instrum. **77**(4), 1–6 (2006)
26. B. Baumann, M. Wolff, B. Kost, H. Groninga, *Proceedings of the COMSOL Users Conference* (2006)
27. B. Baumann, M. Wolff, B. Kost, H. Groninga, Appl. Opt. **46**, 1120–1125 (2007)
28. L.S. Rothman, I.E. Gordon, A. Barbe, D. Chris Benner et al., JQSRT **110**, 533–572 (2009)